An Analytical Model for the Vorticity Associated with a Transverse Jet

A. R. Karagozian*
University of California, Los Angeles, California

A two-dimensional model is developed for a turbulent jet injected normally into a uniform cross flow, in which particular emphasis is placed on the contrarotating vortex pair associated with the jet. By approximating the forces acting on each of the viscous vortices, equations governing vortex spacing and downstream jet velocity are evolved. A description of the variation in total vortex strength is utilized in which vorticity generated by flow about the circular orifice dominates the near field and vorticity generated by the jet impulse dominates the far field. Numerical solution of the governing equations yields results for the vortex trajectory, half-spacing, and varying circulation that correlate quite well with experimental data and asymptotic relations. Based on these findings, it is concluded that vortex separation and other important characteristics of the jet cross section are locally two-dimensional and viscous in nature. Hence, it becomes possible to predict, on largely theoretical grounds, the behavior of the vortex pair and of the transverse jet itself.

Nomenclature

a	= radius of viscous core
d	= orifice diameter
e	= local entrainment factor
f	= complex potential
F_x	= unsteady drag force acting on vortices
F_y	= lift force acting to separate vortices
h	= half-spacing of vortices
k	= virtual mass coefficient for motion of vortex cores
ℓ	= half-height of vortex pair recirculation cell
L	= characteristic length scale for transverse jet
m	= half-width of vortex pair recirculation cell
$\dot{m}_j$	= mass flow rate exiting jet orifice
P	= impluse per unit length of transverse jet
r, r_1, r_2	= radial distances in vortex coordinate system
R	= velocity ratio U_j/U_∞ for isothermal problem
Re	= characteristic Reynolds number ($= U_\infty L/\nu$)
s	= arc length along vortex curve
t	= flow time used to parametrize vortex location
t_o	= initial flow time at jet orifice
$U(t)$	= unsteady cross flow velocity in reference frame of vortex pair
U_j	= jet velocity at orifice
U_∞	= crossflow velocity
u_v	= local mass-averaged velocity of jet along trajectory
X, Y, Z; x_v, y_v, z_v	= coordinate systems relative to wind tunnel and vortex pair, respectively
$\Gamma_0(t)$	= total (integrated) circulation of each vortex
ν	= viscosity
ρ	= density of cross flow and jet
ϕ	= velocity potential
ϕ_v	= angle describing orientation of vortex pair
ω	= vorticity
ω_0	= total (integrated) vorticity associated with each vortex structure

Presented as Paper 84-1662 at the AIAA 17th Fluid Dynamics, Plasma Dynamics and Lasers Conference, Snowmass, CO, June 25-27, 1984; received Jan. 21, 1985; revision received July 8, 1985.

*Assistant Professor, Department of Mechanical, Aerospace and Nuclear Engineering. Member AIAA.

Introduction

THE turbulent mixing of a jet directed normally into a cross flow arises in a variety of situations of technological importance, among them, dilution jet mixing in gas turbine combustion chambers. The practical implications of this flowfield have motivated extensive study of the behavior of the transverse jet, both by experiment and by analysis. While early studies focused on empirical descriptions of the jet trajectory and pressure distribution (Keffer and Baines,[1] Pratte and Baines,[2] Jordinson[3]), more recent experiments have, in addition to jet path, evaluated cross-sectional velocity distributions that indicate the presence of a vortex pair structure dominating the downstream jet flow (Kamotani and Greber,[4] Fearn and Weston[5]). An increase in vortex spacing with downstream distance is observed to occur, as well as an increase in local vortex strength with increasing momentum ratio R^2 (defined as the ratio of the momentum flux of the jet to that of the cross flow over an area equal to that of the jet orifice).

Over the past decade a number of semianalytical models have been developed that place particular emphasis on the vortex pair structure and its behavior in terms of predicting the jet trajectory. The models of Fearn and Weston[5] and of LeGrives[6] assume the vortex pair to be locally two-dimensional and consider the pair to slightly "lag" the actual jet trajectory, which is defined by the location of points of maximum velocity in the jet's plane of symmetry. These assumptions are quite accurate in light of experimental findings, yet empirical information is required as input to each model, particularly that of Fearn and Weston. The two-dimensional, inviscid models of Durando[7] and of Broadwell and Briedenthal[8] consider the vortex pair in the far field to be aligned with the direction of the cross flow, where vorticity originates from the impulse per unit length imparted to the flowfield by the jet. Scaling laws for the vortex trajectory (assumed identical to that of the jet) and the variation in downstream vortex strength are then evolved, based on similarity arguments. While relatively few empirical results are incorporated into these models, the neglect of viscous dissipation and local jet path curvature causes the models to be inappropriate within 50 jet diameters downstream of injection, where much of the experimental work has been performed.

The present model has been developed with the aim of explaining some of the fundamental features of transverse jet

flow and the degree to which simplifying assumptions are appropriate. Specifically, it is sought to determine whether the vortex pair separation and associated increase in jet cross-sectional area are locally two-dimensional or three-dimensional phenomena and whether viscosity must be taken into account in the analysis. The nature of fluid entrainment by the jet is represented in light of these findings, and a prediction of jet trajectory and downstream vortex spacing is obtained.

Description of the Two-Dimensional Model

Experimental observations of the circular jet in a cross flow indicate the presence of a pair of bound vortices initially attached to the lee side of the jet boundary, which gradually dominate the actual jet cross section in the far field. A precise mathematical description of these deflected vortices would consider two semi-infinite, curved vortex lines emanating from points outside of the jet orifice and with image vortex lines represented in the lower wall. The present model, however, considers the vortex pair to be locally two-dimensional, as assumed by previous researchers[5-8] and as is shown in Fig. 1. This assumption is clearly appropriate in the far field of the jet and, for large momentum ratios, is not unreasonable in much of the near field.

Also inherent in the present formulation is the assumption that each vortex structure consists of a Gaussian distribution of vorticity, similar to the "diffuse" vortex model of Fearn and Weston.[5] The concept of the diffusion of vorticity is particularly important to our model in that the downstream growth of each viscous vortex core gives rise to forces that act to separate the vortices.

The geometry of the transverse jet formed by injection into a wind tunnel (or into a combustor) is shown in Fig. 2. The projection of the vortex trajectory onto the plane of symmetry is described by the coordinates $(x_v, y_v = 0, z_v)$ and is defined as the vortex curve. The vortex pair trajectory does in fact "lag" the actual jet path to a degree but, as pointed out by Fearn and Weston[5] and by Adler and Baron,[9] the vortex curve probably coincides more closely with the actual jet path (observed by flow visualization) than does the "jet centerline," the locus of points of maximum velocity.

The concept of a flow time associated with the local (axial) jet velocity is introduced into the model as a means of describing the location of the vortex pair along the vortex curve. In terms of the present model, experiments indicate that, as time increases, the vortices separate further and the viscous cores increase in size. One aim of our model is to predict this separation by analytical arguments, then, based on the geometry of the vortex model, to compute the vortex curve given by $(X, Y = 0, Z)$.

Calculation of the forces acting on the vortex pair arises from an approximation of the cross-sectional velocity distribution of the pair. With respect to the geometry shown in Fig. 3, the vorticity distributions within each of the contrarotating vortices are given by

$$\omega(r_1) = \omega_0 \exp(-r_1^2/4\nu t), \quad \omega(r_2) = -\omega_0 \exp(-r_2^2/4\nu t) \quad (1)$$

Owing to the nature of the radial diffusion of vorticity with time, the flowfield of the single Gaussian viscous vortex is frequently approximated by the Rankine combined vortex. This type of flow concentrates viscous effects into a core region undergoing solid body rotation, with the flowfield of an inviscid (potential) vortex exterior to the core. The velocity distribution for a pair of Rankine combined vortices is

$$v = \begin{cases} \dfrac{\Gamma_0 r_1}{2\pi a^2(t)}\hat{e}_{\theta 1} - \dfrac{\Gamma_0 r_2}{2\pi a^2(t)}\hat{e}_{\theta 2} & \text{for } r_1, r_2 \le a(t) \\ \dfrac{\Gamma_0}{2\pi r_1}\hat{e}_{\theta 1} - \dfrac{\Gamma_0}{2\pi r_2}\hat{e}_{\theta 2} & \text{for } r_1, r_2 \ge a(t) \end{cases} \quad (2)$$

where

$$a(t) = C\sqrt{4\nu t} \quad (C = 1.121)$$

is the radius of the viscous core. Due to the changing orientation of the vortex pair as it is deflected downstream, the cross-flow component seen by the vortex pair will vary with flow time. The two-dimensional flowfield generated by inviscid, unsteady flow about two contrarotating cores of radius $a(t)$ with respective circulations $\pm\Gamma_0$ is shown in Fig. 4. Of course, this approximation is valid when $a(t)$ is less than the vortex half-spacing, $h(t)$; this constraint will be checked upon solution for $a(t)$ and $h(t)$.

The complex potential describing the local flowfield about the vortex with reference to Fig. 4 thus takes the form

$$f(z,t) = U(t)z + U(t)a^2(t)[(1/z) + [1/(z+i2h(t))]] + i\Gamma_0/2\pi[\ln z - \ln(z+i2h(t))] \quad (3)$$

The first term on the right side of Eq. (3) represents the component of uniform flow seen by the vortex pair, the second term represents two circular cylinders (vortex cores) of radius $a(t)$ located at $z = x + iy = 0$ and $z = -i2h(t)$, and the third term represents the circulation of the cylinders $\pm\Gamma_0$ at $z = 0$, $-i2h(t)$, respectively. The components of force that act on each of the cores are F_x and F_y, as shown, representing inviscid, unsteady drag and lift forces, respectively.

Evaluation of the forces F_x and F_y acting on the upper core proceeds from use of the extended Blasius theorem[10] for unsteady, inviscid flow over a body whose size changes with time. In order that the reference frame be fixed to the core, the velocity of each vortex core due to the presence of the adjacent vortex must equal the cross-flow component $U(t)$. Thus,

$$U(t) = U_\infty \sin\phi_v(t) = \Gamma_0/4\pi h(t) \quad (4)$$

Incorporating this velocity balance into the expression for the complex velocity, the resulting components of force become

$$\frac{F_x}{\text{depth}} = \rho\Gamma_0\left[\frac{dh}{dt}\left(1 - \frac{a^2(t)}{2h^2(t)}\right) + \frac{a(t)}{h(t)}\frac{da}{dt}\right] \quad (5a)$$

$$\frac{F_y}{\text{depth}} = \frac{\rho\Gamma_0^2 a^2(t)}{8\pi h^3(t)}\left[1 - \frac{a^2(t)}{4h^2(t)}\right] + \rho\pi a^2(t)\frac{d^2h}{dt^2} \quad (5b)$$

Of particular interest in the calculation of downstream vortex half-spacing $h(t)$ is the lift F_y, which acts to separate the vortex cores. Assuming that ρ, the density of the cross flow, is equal to the density of the jet fluid, and also considering the fluids to be incompressible, the force balance in the y_v direction becomes

$$\frac{d}{dt}\left[\rho(1+k)\pi a^2(t)\frac{dh}{dt}\right] = \frac{F_y}{\text{depth}} \quad (6)$$

The left side of Eq. (6) represents the temporal change in the momentum per unit depth of the core itself, where the term $k\rho\pi a^2(t)$ is the virtual mass of each body that arises due to the change in kinetic energy of the fluid surrounding the core. The virtual mass coefficient k for a moving cylinder with circulation in an unsteady flowfield adjacent to an identical body will necessarily differ from unity. Based on the reasoning described in the Appendix, the value $k = 4$ is chosen in the present calculation and is approximated as constant for the entire vortex pair trajectory. Substitution for the force component F_y into Eq. (6) gives an ordinary dif-

ferential equation in the vortex half-spacing $h(t)$ and in the core radius $a(t)$.

Thus far, no actual viscous information has been incorporated into the model; the cores have been assumed to grow at some general rate $2\pi a(da/dt)$. By definition, the viscous core radius increases with time as $a(t) = C\sqrt{4\nu t}$; this substitution into Eqs. (5b) and (6) yields a single governing equation in vortex half-spacing $h(t)$. The selection of an appropriate viscosity for the turbulent jet in a cross flow, however, requires some care. The implications here may be seen by nondimensionalizing the parameters present in the governing equation for $h(t)$.

As described in Broadwell and Briedenthal,[8] an appropriate length scale for the problem of a transverse jet can be

$$\mathcal{L} = (\dot{m}_j U_j/\rho U_\infty^2)^{1/2} \sim Rd$$

where R reduces to the jet-to-cross-flow velocity ratio (U_j/U_∞) for the incompressible problem. Using a characteristic length $L = Rd$, flowfield parameters may be nondimensionalized as follows: $\tilde{h} = h/L$, $\tilde{t} = U_\infty t/L$; $\tilde{\Gamma}_0 = \Gamma_0/U_\infty L$. The final dimensionless equation for half-spacing $\tilde{h}$ thus becomes

$$\frac{d^2\tilde{h}}{d\tilde{t}^2} + \left(\frac{k+1}{k}\right)\frac{1}{\tilde{t}}\frac{d\tilde{h}}{d\tilde{t}} - \frac{\tilde{\Gamma}_0^2}{8\pi^2 k\tilde{h}^3(\tilde{t})}\left[1 - \frac{C^2\tilde{t}}{(Re)\tilde{h}^2(\tilde{t})}\right] = 0 \tag{7}$$

where the Reynolds number for the flowfield is defined by

$$Re = \frac{U_\infty L}{\nu} = \frac{U_j d}{\nu} \text{ (incompressible)}$$

Now the Reynolds numbers (based on kinematic viscosity) prevalent in experimental studies range from the order of 10^3-10^4 for the heated jet in a cross flow (Kamotani and Greber[4]) to 10^6 for the isothermal work of Fearn and Weston.[5] If eddy viscosity is instead employed in the definition of Re [and thus in the relation for $a(t)$], the pertinent Reynolds numbers for the experiments will be reduced by perhaps several orders of magnitude. Hence, several different values of Re will be considered in calculation for the present model in order to assess the effects of viscosity selection.

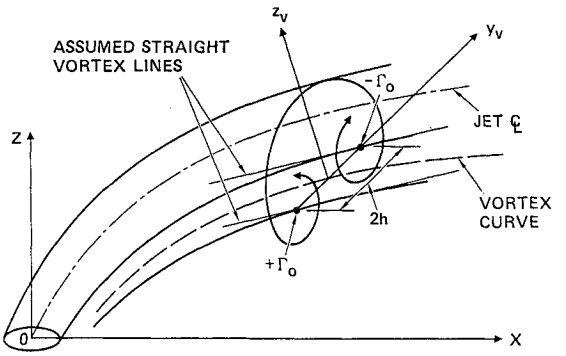

Fig. 1 Description of a locally two-dimensional vortex pair in the field of a transverse jet.

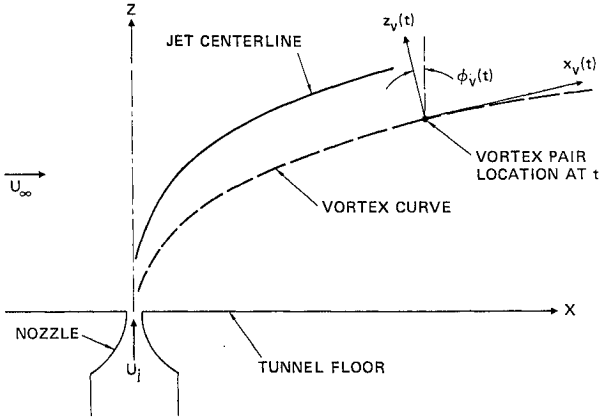

Fig. 2 Geometry for a two-dimensional model.

Solution of the nonlinear ordinary differential equation given in Eq. (7) is now contingent upon formulation of several important quantities: Γ_0, the total (integrated) circulation associated with each vortex, and the initial conditions for $\tilde{h}(\tilde{t})$ and for $d\tilde{h}/d\tilde{t}$ at the jet orifice. In evaluating the relationship between Γ_0 and other parameters describing the transverse jet, it is necessary to postulate in some detail how the vorticity is actually generated in the flow and to understand what is actually observed in the cross-sectional slices of the jet taken experimentally. Historically, it has been assumed that the rollup of vorticity arising from two-dimensional flow about a circular orifice is a fairly reasonable means of visualizing the formation of the pair of contrarotating vortices.[11] If the interaction of the cross flow with the circular jet orifice were the only means by which the vortex pair is formed, however, then 1) the orientation of the vorticity vectors would be perpendicular to the direction of cross flow, and 2) the circulation of each vortex would be virtually independent of the jet-to-cross-flow momentum ratio, $R^2 = \rho U_j^2/\rho U_\infty^2$. Jet cross-section velocity data[4,5] indicate, however, that integrated vortex strength does increase with this ratio and that Γ_0 generally increases then decreases with arc length along the vortex curve. Hence, to model the circulation more accurately, particularly in the downstream region, the component of vorticity generated by the impulse of the jet must be included. Durando,[7] following the description of Lamb,[12] gives the impulse per unit length P necessary to generate a vortex pair instantaneously from rest as

$$\boldsymbol{P} = (2\rho\Gamma_0 h)\hat{k} \tag{8}$$

In this description the two vortex lines are parallel to the direction of cross flow, and in fact this relation for Γ_0 is used in the far-field models of Durando[7] and of Broadwell and Breidenthal.[8]

One means of accounting for both components of the vorticity generated at the orifice is to express the circulation as

$$\Gamma_0 = [2U_\infty d]\sin\phi_v(t) + [P/2\rho h(t)]\cos\phi_v(t) \tag{9}$$

where the coefficient of $\sin\phi_v(t)$ represents the vortex strength generated by the cross flow and the coefficient of $\cos\phi_v(t)$ represents the circulation arising from the jet impulse. The impulse per unit depth of the jet is given by

$$P = \dot{m}_j U_j/U_\infty = \rho\pi d^2 U_j^2/4U_\infty$$

for the case where the densities of the fluids are the same. The dimensionless representation for Γ_0 can then be written (using the cross-flow velocity balance) as

$$\tilde{\Gamma}_0(\tilde{t}) = (\pi^2/2)\Big/\sqrt{\left(4\pi\tilde{h} - \frac{2}{R}\right)^2 + \left(\frac{\pi}{8\tilde{h}(\tilde{t})}\right)^2} \tag{10}$$

This relation indicates that $\tilde{\Gamma}_0$ is actually a function of dimensionless flow time $\tilde{t}$ in Eq. (7), appropriate in that near-field and far-field vorticity components dominate in different portions of the jet trajectory. In the actual numerical solution of Eq. (7), however, the term $\tilde{\Gamma}_0$ will be regarded as quasi-steady, with the numerical value of $\tilde{\Gamma}_0$ updated at successive time intervals based on $\tilde{h}(\tilde{t})$. Since the expression in Eq. (10) is an externally imposed correlation

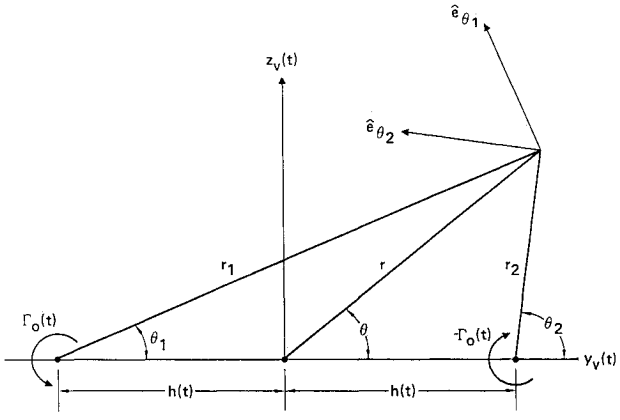

Fig. 3 Geometry for local flowfield of vortex pair.

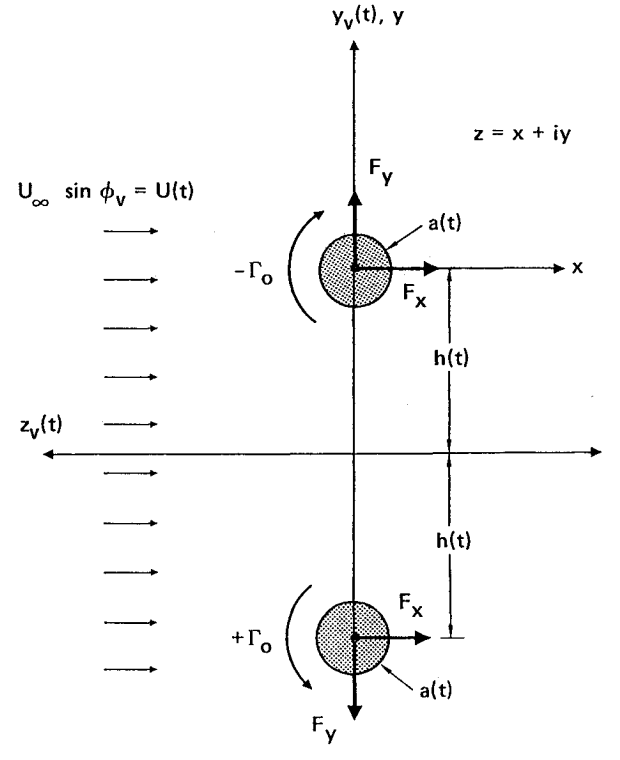

Fig. 4 Local flowfield and forces acting on viscous cores.

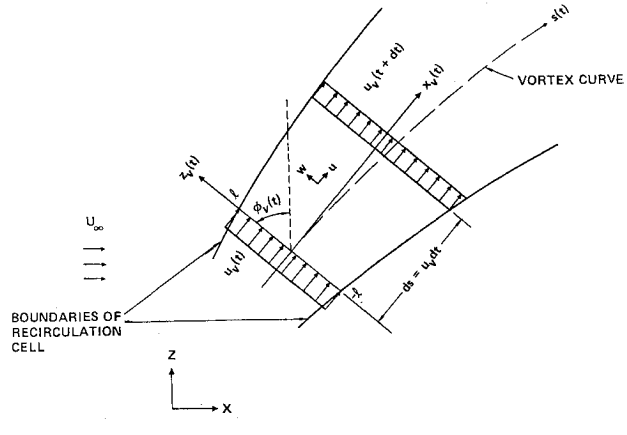

Fig. 5 Flowfield relative to an element of the vortex pair recirculation cell.

(albeit with analytical justification) and not a part of the unsteady force calculation, it is reasoned that this simplification in the numerical analysis is acceptable.

The value of the dimensionless vortex half-spacing $\tilde{h}(\tilde{t})$ at the jet orifice (and hence at an "initial" flow time $\tilde{t}_o$) is difficult to determine, in both theory and experiment. Clearly, if the situation near the jet orifice is modeled as flow about a circular cylinder, the attached vortex pair that is formed will have nonzero half-spacing.

As one means of approximating $\tilde{h}(\tilde{t}_o)$, the assumption is made that the cross-sectional area of the recirculation cell of the vortex pair is equal to the area of the jet orifice. This is based on the reasoning that, further downstream of the orifice, the recirculation cell of the vortex pair becomes more closely representative of the actual jet cross section. If extrapolated back to the location of the orifice, this gives

$$\tilde{h}(\tilde{t}_o) = (1/R)\sqrt{\pi/16B} \tag{11}$$

with $B = 2.84$ evaluated by the dimensions of the cell (Kelvin oval) given in Robertson.[13]

The actual time $\tilde{t}_o$ to which this value of $\tilde{h}(\tilde{t}_o)$ corresponds is evaluated by an asymptotic solution of the governing equation for $\tilde{h}(\tilde{t})$. If we assume that $\tilde{t}_o$ is close to zero and that $\tilde{h}(\tilde{t}) \sim \tilde{t}^{\gamma}$ near $\tilde{t} = 0$, the first-order dependence of $\tilde{h}(\tilde{t})$ is found by substitution into Eq. (7). This yields

$$\tilde{h}(\tilde{t}) = b\tilde{t}^{1/2} \tag{12}$$

as an approximation to the function close to zero. The coefficient b is computed easily by neglecting the term of order $(1/Re)$ in Eq. (7). Hence, given the value for $\tilde{h}(\tilde{t}_o)$ in Eq. (11), the corresponding flow time $\tilde{t}_o = (\tilde{h}(\tilde{t}_o)/b)^2$ may be calculated, and the initial rate of change of the spacing, which is also required, is simply equal to $(b/2)\tilde{t}_o^{-1/2}$. The initial conditions for Eq. (7) are now complete and the equation is ready for numerical solution.

Once the solution for dimensionless downstream half-spacing $\tilde{h}(\tilde{t})$ is obtained, it can be used to calculate the vortex curve $Z(X)$. From the velocity balance along the trajectory, it is clear that the geometrical relationship between the local slope of the trajectory, dZ/dX, and the local vortex half-spacing is

$$\frac{dZ/dX(t)}{[1+(dZ/dX(t))^2]^{1/2}} = \sin\phi_v(t) = \frac{\tilde{\Gamma}_0(\tilde{t})}{4\pi\tilde{h}(\tilde{t})} \tag{13}$$

Based on the definitions here, the arc length of the vortex curve at flow time $\tilde{t}$ is given by the time integral of the local mass-averaged jet velocity, $u_v(t)$. In dimensionless form, $\tilde{u}_v = u_v/U_j$ and arc length can be represented by

$$\frac{s(\tilde{t})}{d} = \int_{\tilde{t}_o}^{\tilde{t}} \tilde{u}_v(\tau)\,d\tau \tag{14a}$$

then, correspondingly, the location of the vortex pair at t is $(X(t), Z(t))$, where

$$\frac{X(\tilde{t})}{d} = R^2 \int_{\tilde{t}_o}^{\tilde{t}} \tilde{u}_v(\tau)\cos\phi_v(\tau)\,d\tau \tag{14b}$$

$$\frac{Z(\tilde{t})}{d} = R^2 \int_{\tilde{t}_o}^{\tilde{t}} \tilde{u}_v(\tau)\sin\phi_v(\tau)\,d\tau \tag{14c}$$

Once the functions $\tilde{h}(\tilde{t})$ and $\tilde{\Gamma}_0(\tilde{t})$ are numerically evaluated at specific values of dimensionless time, the above integrals can also be evaluated numerically to produce the vortex curve. We have yet to compute the local average of the axial velocity of the fluid in the recirculation cell, $u_v(t)$.

Figure 5 describes in two dimensions the flow entering and exiting an element of the vortex pair recirculation cell in the x_v-z_v plane. The actual area of the cell, $4Bh^2(t)$, increases along the vortex curve, and the length of the cell is given by $ds = u_v dt$. The equations governing behavior of the three-dimensional velocity field within the cell are the incompressible continuity equation and x_v component of conservation of momentum, given, respectively, by

$$\frac{\partial u}{\partial x_v} + \frac{\partial v}{\partial y_v} + \frac{\partial w}{\partial z_v} = 0 \tag{15a}$$

$$\frac{\partial (u^2)}{\partial x_v} + \frac{\partial (uv)}{\partial y_v} + \frac{\partial (uw)}{\partial z_v} = \frac{\partial}{\partial z_v}(\tau_{zx}) \tag{15b}$$

This preliminary assessment neglects pressure variation along the vortex curve and will neglect shearing stresses at the cell boundaries. Combining these two equations into one, and integrating over the area of the cell, Liebnitz' rule gives the relation

$$\frac{d}{dx_v}\left\{\int_{-m}^{m}\int_{-\ell}^{\ell} u^2 dz_v dy_v\right\} - U_\infty \cos\phi_v(t)\frac{d}{dx_v}\left\{\int_{-m}^{m}\int_{-\ell}^{\ell} u dz_v dy_v\right\} = 0 \tag{16}$$

where 2ℓ and $2m$ are the height and width of the cell, respectively. The limits $u(\pm\ell) = U_\infty \cos\phi_v(t)$ have been used to represent the component of cross flow in the x_v direction seen by the fluid exterior to the recirculation cell. Approximating the velocity in the cell as a mass-averaged quantity $u_v(t)$, and rewriting Eq. (16) for an element of length ds, the dimensionless governing equation for $\tilde{u}_v$ emerges:

$$\frac{d\tilde{u}_v}{d\tilde{t}} = \frac{[\cos\phi_v(\tilde{t}) - R\tilde{u}_v(\tilde{t})]}{[2R - \cos\phi_v(\tilde{t})/\tilde{u}_v(\tilde{t})]}\frac{2}{\tilde{h}(\tilde{t})}\frac{d\tilde{h}}{d\tilde{t}} \tag{17}$$

where

$$\cos\phi_v(\tilde{t}) = \sqrt{1 - (\tilde{\Gamma}_0(\tilde{t})/4\pi\tilde{h}(\tilde{t}))^2}$$

Hence, knowledge of the function $\tilde{h}(\tilde{t})$ and $\tilde{\Gamma}_0(\tilde{t})$ allows solution of the nonlinear ordinary differential equation (17). The initial condition at the orifice is given by $\tilde{u}_v(\tilde{t}_o) = 1.0$. It can be seen that in the limit as $\cos\phi_v(\tilde{t})$ approaches unity, the change in $\tilde{u}_v$ with dimensionless flow time vanishes when $\tilde{u}_v$ approaches the reciprocal of the velocity ratio, $1/R = U_\infty/U_j$, which is an appropriate far field condition.

Results and Comparison with Experiment

In order to obtain the predicted vortex curve, the half-spacing as a function of downstream distance, and other results for comparison with experimental data, the governing equations (7) and (17) are solved, subject to relation (10) and to the pertinent initial conditions. Equation (7) for $\tilde{h}(\tilde{t})$ is to be evaluated first, using a fourth-order Runge-Kutta scheme. Since the magnitude of the initial condition $(d\tilde{h}/d\tilde{t})(\tilde{t}_o)$ could cause an instability in the numerical solution, however, further nondimensionalization of Eq. (7) with respect to the asymptotic solution is required before the numerical analysis can be performed. This is done by defining a new dependent variable

$$\hat{h}(\tilde{t}) = \tilde{h}(\tilde{t})/b\tilde{t}^{1/2} \tag{18}$$

and transforming the differential equation (7) and its initial conditions. The new equation in $\hat{h}(\tilde{t})$ is then solved numerically and values of $\tilde{h}(\tilde{t})$ and $d\tilde{h}/d\tilde{t}$ can be derived from $\hat{h}(\tilde{t})$. With these results, Eq. (17) can then be solved using the Runge-Kutta scheme. Finally, the position of the vortex pair corresponding to a given dimensionless flow time $\tilde{t}$ is computed by numerical integration of Eqs. (14a-14c).

Results for the predicted vortex curve for different values of the velocity ratio $R = U_j/U_\infty$ are shown in Fig. 6a, with Reynolds number Re taken to be equal to 1000. The experimental points indicated are those based on the work of Kamotani and Greber[4] and of Thompson,[14] with the rest calculated from a least-squares fit of the data from Fearn and Weston.[5] In general, the power law that describes the shape of the curve is of the form

$$Z/d = \alpha_1 (R)^{\beta 1} (X/d)^{\gamma 1} \tag{19}$$

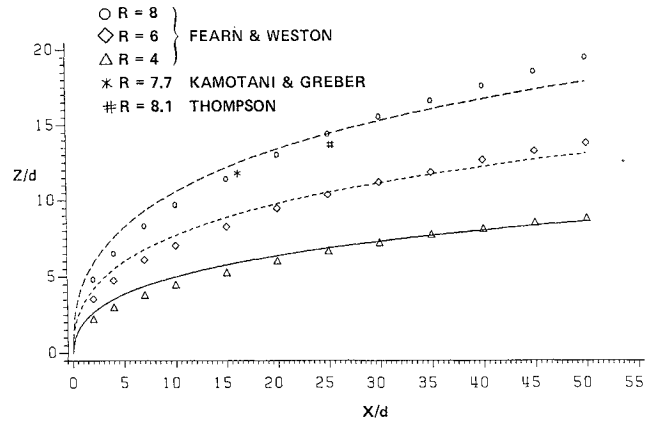

Fig. 6a Vortex pair trajectories for $R=8$ (– – –), 6 (-----), 4 (———) at Reynolds number $Re=10^3$.

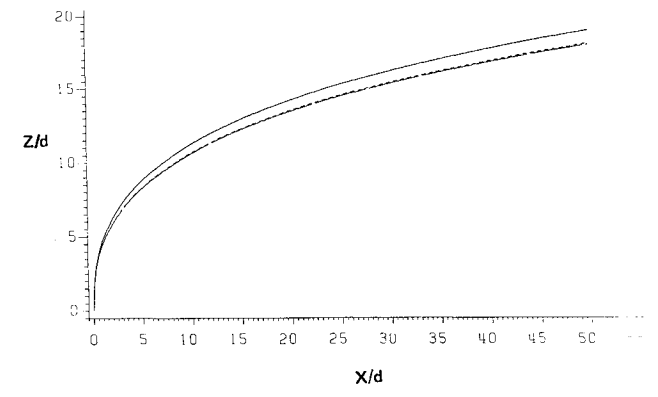

Fig. 6b Vortex pair trajectories for Reynolds numbers $Re=10^2$ (———), 10^3 (-----), 10^4 (– – –), at $R=U_j/U_\infty=8$.

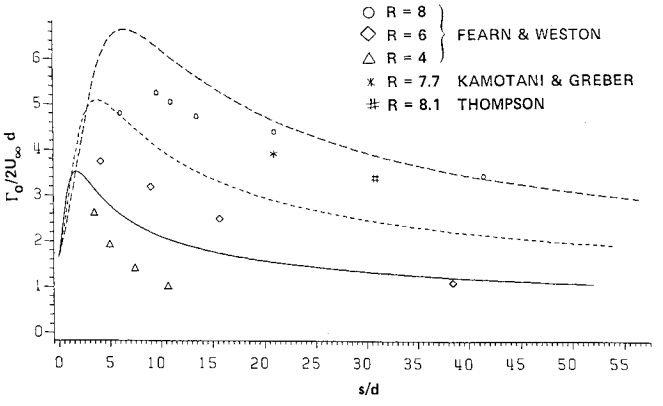

Fig. 7 Dimensionless circulation vs dimensionless arc length for $R=U_j/U_\infty=8$ (– – –), 6 (-----), 4 (———), at Reynolds number $Re=10^3$.

The values of the constants from Fearn and Weston's semiempirical data are $\alpha_1 = 0.3473$, $\beta_1 = 1.127$, $\gamma_1 = 0.4291$; the far-field (i.e., beyond 50 jet diameters downstream) experiments of Pratte and Baines[2] give $\alpha_1 = 2.05$, $\beta_1 = 0.72$, and $\gamma_1 = 0.28$, and the analysis of Broadwell and Breidenthal[8] gives $\beta_1 = 0.67$ and $\gamma_1 = 0.33$. Our results give, as an approximation over the entire curve to $X/d = 50$, $\alpha_1 = 0.527$, $\beta_1 = 1.178$, and $\gamma_1 = 0.314$. For purposes of comparison, the quantity that is most important is the value of γ_1, the exponent of the term X/d, since α_1 and β_1 are largely dependent on the initial conditions chosen.

The dependence of these results on Reynolds number is shown in Fig. 6b, with the chosen range of Re based on both kinematic viscosity and eddy viscosity values. For comparison with the Fearn and Weston[5] experiments, it is clear that even if appropriate eddy viscosities are three to four orders of magnitude greater than the actual kinematic quantity (i.e., comparing results for $Re = 10^2$ or 10^3 with $Re = 10^6$), the effects on the model are not very significant. In fact, for Reynolds numbers above 10^3, the effect of Re on the results is negligible. Thus, while the inclusion of viscosity is essential to the nature of the model itself (via vortex separation), the actual selection of the viscosity coefficient ν is not critical.

A dimensionless form of integrated vortex strength, $\Gamma_0/2U_\infty d$, is plotted as a function of the dimensionless arc length s/d in Fig. 7. By comparison with experiments and with semiempirical results, the vortex strength obtained in the vicinity of the jet orifice undergoes a very dramatic increase, but then decreases beyond $s/d = 3$ to 5. Downstream of $s/d = 20$, the power law describing integrated vortex strength is

$$\Gamma_0/2U_\infty d = \alpha_2 (R)^{\beta_2} (X/d)^{\gamma_2} \tag{20}$$

where our calculations give $\alpha_2 = 0.469$, $\beta_2 = 1.631$, and $\gamma_2 = -0.38$ compared with the far field values $\beta_2 = 1.33$, $\gamma_2 = -0.33$ obtained by Broadwell and Breidenthal. The increase in Γ_0 in the near field is observed to a small degree in experiments, as shown in Fig. 7. But, in actuality, the predicted behavior of Γ_0 indicates that circulation is not really a slowly varying function of time near the orifice. However, the locally two-dimensional assumption for performing the entire analysis is less accurate in the vicinity of the orifice; thus, since the current evaluation method for $\Gamma_0(t)$ and for the orifice conditions employed is quite sufficient to produce appropriate downstream behavior, relation (9) will continue to be considered reasonable.

Dimensionless vortex half-spacing is shown in Fig. 8. Although the differences among the three different cases for velocity ratios are small, the general empirical trend, where spacing increases with velocity ratio, is observed. Experimental points shown indicate that the predicted values of h/d are roughly of the same size. In fact, the far field (asymptotic) behavior of the vortex pair, described by

$$h/d = \alpha_3 (R)^{\beta_3} (X/d)^{\gamma_3} \tag{21}$$

is fairly reasonable in that we obtain $\alpha_3 = 1.50$, $\beta_3 = 0.27$, and $\gamma_3 = 0.37$ compared with $\beta_3 = 0.67$, $\gamma_3 = 0.33$ from Broadwell and Breidenthal.[8]

Entrainment of cross flow is represented in the present model by the increase in the size of the vortex pair recirculation cell due to vortex separation. One means of expressing local entrainment in this isothermal situation is through the local rate of increase in cell area, represented nondimensionally by

$$e = \left(\frac{d}{Q_o}\right)\frac{dQ}{ds} = \left(\frac{16Bb^2}{\pi \bar{u}_v}\right)\frac{d}{dt}(\tilde{t}\tilde{h}^2(\tilde{t})\tilde{u}_v(\tilde{t})) \tag{22}$$

where Q is the local volume flux of fluid in the jet (or cell) and Q_o is the volume flux at the orifice. When evaluated as a function of dimensionless downstream distance X/d, the local entrainment factor e increases, then decreases, as shown in Fig. 9, and the term also increases in the far field with velocity ratio R. This result is appropriate in that the degree of mixing in the flow, indicated by vortex strength Γ_0, also reaches a maximum, then decreases downstream.

Finally, a check is made on the assumption that core radius $a(t)$ is less than vortex half-spacing $h(t)$. Figure 10 describes this comparison in nondimensional terms, for

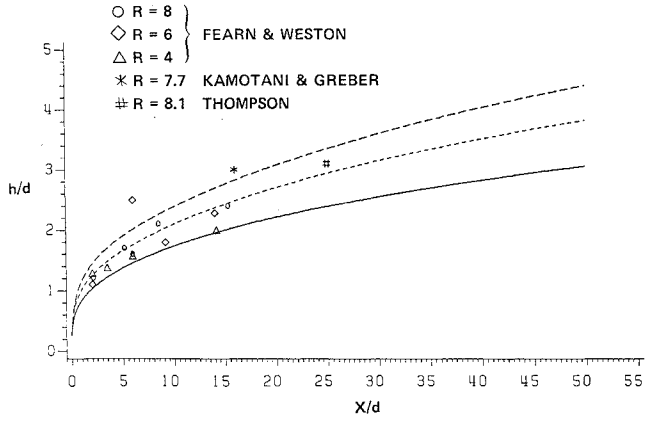

Fig. 8 Dimensionless vortex half-spacing vs dimensionless downstream distance for $R = U_j/U_\infty = 8$ (– – –), 6 (-----), 4 (———), at Reynolds number $Re = 10^3$.

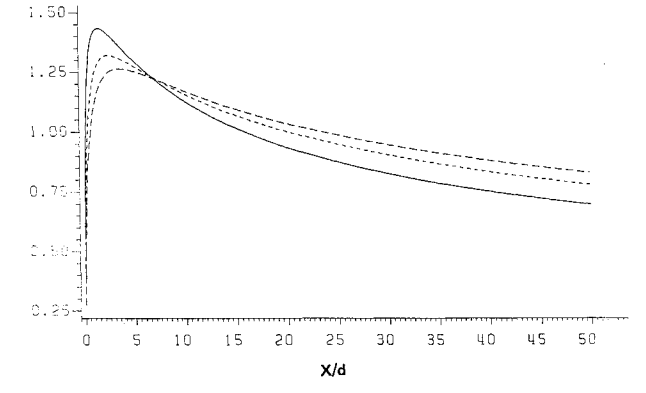

Fig. 9 Entrainment coefficient e as a function of a dimensionless downstream distance for $R = U_j/U_\infty = 8$ (– – –), 6 (-----), 4 (———), at Reynolds number $Re = 10^3$.

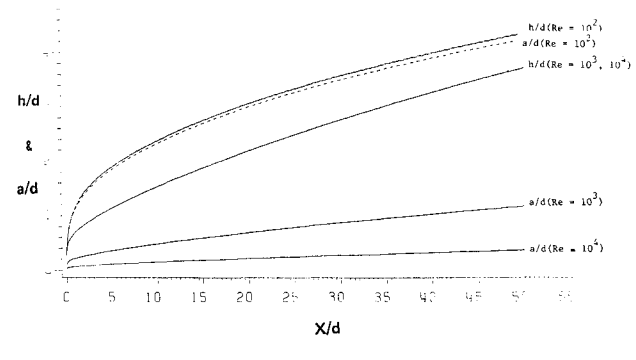

Fig. 10 Comparison of dimensionless vortex half-spacing h/d and viscous core radius a/d as a function of dimensionless downstream distance for Reynolds numbers $Re = 10^2$, 10^3, and 10^4, and $R = U_j/U_\infty = 8$.

several different values of the Reynolds number. As expected, in the lower Reynolds number cases ($Re=100$), the magnitude of $a(t)$ is close to but still lower than $h(t)$. As Reynolds number is increased to values of 1000 and above, $a(t)$ is quite a bit smaller than half-spacing $h(t)$ and, thus, for the range of viscosities appropriate to the problem, this fundamental assumption is valid.

Conclusions

The results of this model indicate that vortex pair separation in the flowfield of a transverse jet is largely a two-dimensional, viscous phenomenon. The nature of this separation may be used to predict the trajectory of the vortex pair, but initial conditions in the vicinity of the jet orifice must be formulated such that reasonable downstream characteristics are observed. Since the two-dimensional analysis is not as appropriate in this region, estimation and extrapolation back to the orifice is employed, which works quite well here. In addition, the model for integrated vortex strength presently used indicates that it is reasonable to consider the vorticity generated by the impulse of the jet to dominate the far-field flow, and the vorticity arising from the interaction of cross flow with jet fluid to be significant near the jet orifice. This description reinforces Fearn and Weston's[5] conclusion that the vortices are formed very close to the jet orifice, but asserts that the dependence of two-dimensional vortex strength on jet velocity does not become important until the jet has been deflected by the cross flow.

Appendix: Determination of the Virtual Mass Coefficient

Incorporation of the virtual mass coefficient k in the analysis represents the presence of unsteady forces required to accelerate the surrounding fluid when the cores separate at velocity dh/dt. While the value of k for a single circular cylinder moving in a still fluid is found to be unity, computation of k for the motion of the circular cores in the present case is far more complicated. The present analysis will serve as a means only to approximate k, since there are *two* bodies in motion that grow radially in time with associated circulations $\pm\Gamma_0$ and with a cross flow $U(t)=U_\infty \sin\phi_v(t)$ that does not vanish at an infinite distance from the cores. Thus, the frame of reference of the actual situation (represented in Fig. 4) must be altered so that the core under examination moves in a still fluid. By a superposition of $U(t)$, which places the cores in a stationary fluid, and by inclusion of an "image" wall to represent the lower core, the rate of change of kinetic energy of the flow associated with upper-core motion may be computed:

$$\boldsymbol{U}\cdot\boldsymbol{F}=-\frac{1}{2}\rho\frac{d}{dt}\int_{S_b}\phi\hat{n}\cdot\boldsymbol{v}\,dS+\frac{1}{2}\rho\frac{d}{dt}\int_{S_\Delta}\phi\hat{n}\cdot\boldsymbol{v}\,dS \quad \text{(A1)}$$

In this equation, S_b represents the surface boundary of the upper core and S_Δ represents the semicircular area bounded below by the image wall and extending radially in the upper half-plane to infinity. The velocity field $\boldsymbol{v}$ and potential ϕ for the motion of the core (at velocity $\boldsymbol{U}$) in a still fluid can be written in terms of body-referenced quantities and coordinates, $\phi=\hat{\phi}+\hat{\boldsymbol{x}}\cdot\boldsymbol{U}$, $\boldsymbol{v}=\hat{\boldsymbol{v}}+\boldsymbol{U}$, causing the second integral in Eq. (A1) to vanish since $\boldsymbol{v}=0$ at infinity and since the unit normal vector is perpendicular to $\boldsymbol{v}$ at the image wall.

Substitution of the body-referenced functions into Eq. (A1) now allows an integral equation for the rate of change of kinetic energy to emerge. Evaluation of the equation involves a considerable amount of complicated but straightforward manipulation, the details of which are omitted here. When the substitution $U(t)=\Gamma_0(t)/4\pi h(t)$ is made, core motion in the x direction is eliminated. Finally, when terms of order $(a/h)^4\sim(1/Re)^2$ and higher are neglected, a time-dependent relation for the apparent force F_y in the y direction is obtained. If the virtual mass coefficient k is considered constant for all time (and thus for the entire trajectory of the jet), the value of k can be computed explicitly from the expression for F_y. Written in terms of nondimensionalized variables $\tilde{h},\tilde{t}$, etc., as done in the main text of this paper, the final relation for k reduces to

$$k=\frac{d}{d\tilde{t}}\left\{\tilde{\Gamma}_0\left[\left(\frac{\tilde{\Gamma}_0}{4\pi\tilde{h}}\right)^2+\left(\frac{d\tilde{h}}{d\tilde{t}}\right)^2\right]^{1/2}\frac{\tilde{t}}{4\tilde{h}}+\pi\tilde{t}\left[\left(\frac{\tilde{\Gamma}_0}{4\pi\tilde{h}}\right)^2+\left(\frac{d\tilde{h}}{d\tilde{t}}\right)^2\right]\right\}\div 2\pi\left\{\left(\frac{d\tilde{h}}{d\tilde{t}}\right)^2+\tilde{t}\left(\frac{d\tilde{h}}{d\tilde{t}}\right)\left(\frac{d^2\tilde{h}}{d\tilde{t}^2}\right)\right\} \quad \text{(A2)}$$

Hence, the actual motion of the viscous core, described nondimensionally through $\tilde{h}(\tilde{t})$, can be used to estimate k, the fraction of the mass of the core that arises due to the change in the kinetic energy of the surrounding fluid. However, since the motion of the cores depends on location along the jet trajectory, the virtual mass coefficient is not, strictly speaking, a constant. The approximation for k given in Eq. (A2) can only be used to estimate analytically a value of k in the vicinity of the orifice. Then, presuming that k will increase and then decrease along the trajectory just as the strength of the vortices Γ_0 increases and then decreases, a reasonable estimate of k can be made.

The asymptotic behavior of $\tilde{h}(\tilde{t})$ near the jet orifice has been described in the text as $\tilde{h}=b\tilde{t}^{1/2}$, where b depends on the local circulation, the vortex spacing, and the virtual mass coefficient. If this approximation for $\tilde{h}(\tilde{t})$ is used in Eq. (A2), in addition to an asymptotic relation for $\tilde{\Gamma}_0(\tilde{t})$, a single equation for k emerges:

$$K=\left\{\left(\frac{1}{2}k+1\right)\left[1+\frac{1}{(\frac{1}{2}k+1)}\right]^{1/2}-\frac{1}{2}\left[1+\frac{1}{(\frac{1}{2}k+1)}\right]^{-1/2}+\left(\frac{1}{2}k+1\right)\right\} \quad \text{(A3)}$$

Iterative solution of Eq. (A3) yields $k\cong 2.2$ at the jet orifice. Assuming that k will increase and then decrease along the trajectory, a suitable value of $k>2.2$ must be selected as an average. A number of different values of k can be tried in the calculation, giving roughly similar results for jet trajectories. A value of $k=4$ actually gives results that roughly fit experimentally obtained trajectories; hence, the value $k=4$ is used here, more or less as a fit parameter, but justified by the analysis above to exceed unity.

Acknowledgments

This work was supported by NASA Lewis Research Center under Grant NAG 3-543. The author wishes to acknowledge helpful discussions with Prof. I. Greber of Case Western Reserve University.

References

[1]Keffer, J. F. and Baines, W. D., "The Round Turbulent Jet in a Cross-Wind," *Journal of Fluid Mechanics*, Vol. 15, Pt. 4, 1963, pp. 481-496.

[2]Pratte, B. D. and Baines, W. D., "Profiles of the Round Turbulent Jet in a Cross Flow," *Proceedings of ASCE, Journal of the Hydraulics Division*, Nov. 1967, pp. 56-63.

[3]Jordinson, R., "Flow in a Jet Directed Normal to the Wind," British Aeronautical Research Council, R&M 3074, Oct. 1956.

[4]Kamotani, Y. and Greber, I., "Experiments on a Turbulent Jet in a Cross Flow," *AIAA Journal*, Vol. 10, Nov. 1972, pp. 1425-1429.

[5]Fearn, R. and Weston, R. P., "Vorticity Associated with a Jet in a Cross Flow," *AIAA Journal*, Vol. 12, Dec. 1974, pp. 1666-1671.

[6]Le Grives, E., "Mixing Process Induced by the Vorticity Associated with the Penetration of a Jet into a Cross Flow," *Journal of Engineering for Power*, Vol. 100, July 1978, pp. 465-475.

[7]Durando, N. A., "Vortices Induced in a Jet by a Subsonic Cross Flow," *AIAA Journal*, Vol. 9, Feb. 1971, pp. 325-327.

[8]Broadwell, J. E. and Breidenthal,, R. E., "Structure and Mixing of a Transverse Jet in Incompressible Flow," *Journal of Fluid Mechanics*, Vol. 148, 1984, pp. 405-412.

[9]Adler, D. and Baron, A., "Prediction of a Three-Dimensional Circular Turbulent Jet in Crossflow," *AIAA Journal*, Vol. 17, Feb. 1979, pp. 168-174.

[10]Milne-Thomson, L. M., *Theoretical Hydrodynamics*, 5th ed., The Macmillan Company, New York, 1968, p. 255.

[11]Chang-Lu, H., "Aufrollung unes Zylindrischen Strahles durch Ouerwind," Ph.D. Dissertation, University of Gottingen, 1942.

[12]Lamb, H., *Hydrodynamics*, 6th ed., Dover Publications, New York, 1945, p. 221.

[13]Robertson, J. M., *Hydrodynamics in Theory and Application*, Prentice-Hall, Englewood Cliffs, NJ, 1965, p. 230.

[14]Thompson, A. M., "The Flow Induced by Jets Exhausting Normally from a Plane Wall into an Airstream," Ph.D. Thesis, University of London, 1971.